Electron diffusion in a low pressure methane detector for particle dark matter

M.J. Lehner, K.N. Buckland, G.E. Masek

Department of Physics, University of California San Diego, La Jolla, CA 92093-0319, USA

Abstract

Measurements of the transverse diffusion of drifted electrons in low pressure (19–95 torr) methane are presented. The transverse diffusion coefficient was determined both with and without a magnetic field oriented parallel to the drift, and the expected functional dependence of the diffusion coefficient on pressure, reduced electric field, and magnetic field is demonstrated. These results are then used to show that ionization tracks in a time projection chamber to be used in a particle dark matter search can be drifted distances exceeding 1 m while maintaining resolution better than 1 mm. © 1997 Elsevier Science B.V.

PACS: 95.35.+d; 51.20.+d; 29.40.Gx

1. Introduction

There is considerable experimental evidence that as much as ninety percent of the mass of the Galaxy is in some unseen and as yet undetected form [1]. A leading candidate for this so-called dark matter is the weakly interacting massive particle (WIMP) [2], and several experiments using a variety of techniques [3,4] have been undertaken to detect these particles in recent years. Most of these techniques rely upon the detection of nuclear recoils generated by WIMP–nucleon elastic scattering. Using a gas as a target has several advantages [5,6] over liquid and solid targets, mainly the ability to determine the recoil direction. Due to the rotation of the Earth as it moves through the Galaxy, there will be a diurnal modulation in the average recoil direction which can be used as a means to discriminate between WIMP induced nuclear recoils and background due to neutron–nucleon

scattering.

A time projection chamber (TPC) can be used to measure the energy and direction of a recoiling nucleus, and such a detector is described in detail in [5]. In summary, the detector consists of a 114 cm long by 40 cm diameter cylindrical gas volume. The electrons liberated by the ionization of the gas by a recoiling nucleus are drifted to a sense plane at the end of the chamber by an electric field directed parallel to the cylindrical axis. The sense plane can consist of either a multiwire proportional counter, a parallel plate avalanche chamber with optical readout, or any other device capable of detecting ionization as a function of position. Because the typical recoil energies are on the order of a few to a few hundred keV, the pressure of the target gas must be reduced in order to extend the ranges of the recoils to lengths exceeding the resolution of the detector. This will reduce the total target mass, so one would like to have the largest possible

target gas volume. Therefore, a large drift distance is desired, and the effects of electron diffusion during the drift to the sense plane must be minimized in order to maintain the integrity of the ionization track so that the recoil direction may be accurately determined.

A point source distribution of electrons, after being drifted a distance L in the z direction by an electric field E, will diffuse in the x–y plane into a distribution of the form [7]

$$\frac{d^2N}{dxdy} \propto e^{-(x^2+y^2)/2\sigma^2}, \tag{1}$$

where the diffusion width σ is given by

$$\sigma = \sqrt{2D\frac{L}{W}}. \tag{2}$$

Here W is the electron drift velocity and D is the diffusion coefficient, given by

$$D = \frac{vl}{3}, \tag{3}$$

where l is the electron mean free path and v is the mean electron velocity.

The standard TPC configuration includes a magnetic field oriented parallel to the drift field to reduce the diffusion width σ. The transverse diffusion coefficient in a magnetic field B is given by [7]

$$D(B) = \frac{D(B=0)}{1 + \omega^2\tau^2}, \tag{4}$$

where $\omega = eB/m$ is the electron cyclotron frequency (e and m are the charge and mass of an electron) and $\tau = l/v$ is the electron mean collision time. Note that the magnetic field has no effect on the longitudinal diffusion coefficient which becomes so large at lower pressures that no useful timing information can be obtained. Therefore, only a two-dimensional projection of the recoil direction can be determined. However, this is still sufficient to provide discrimination between a WIMP signal and a neutron background [6].

In the following sections, measurements of the diffusion width σ, the drift velocity W, the diffusion coefficient D, and the electron mean collision time τ are presented as functions of pressure P, reduced electric field $K = E/P$, and magnetic field B. It is then shown that the diffusion width σ can be reduced to less than 1 mm after drifting the entire 114 cm length of the TPC when placed in a 4.5 kG magnetic field.

2. Apparatus

The device used here is a modified version of an apparatus used in an earlier experiment [8], and a schematic can be seen in Fig. 1. Drift electrons are created by aiming a pulsed ultraviolet laser (337 nm) through a fused silica window and onto a low work function, high quantum efficiency photoelectric surface (2,2'-binaphthyl [9]). The emitted electrons are drifted through a 0.343 mm aperture into the drift volume and down to a proportional counter by high voltages applied to the photoelectric surface and the top of the drift region. A field cage consisting of a series of copper rings is used to provide a uniform electric field from the entrance aperture to the proportional counter, and the high voltages are set to balance the electric fields on either side of the aperture. The proportional counter consists of a moveable stage with a 20 μm sense wire directly below a 0.305 mm slit. The counter can be moved in a direction perpendicular to the sense wire by a linear motion feedthrough so that the number of electrons passing through the slit can be counted at a number of different slit positions. To explore the effects of a magnetic field on the diffusion width, the entire apparatus is placed between the pole faces of an electromagnet ($B = 3.89$ kG) with the field oriented parallel to the drift field. To insure gas purity, the device is connected to a continuously flowing gas system designed to set the gas pressure in a range of 10 to 100 torr. The drift time is measured by the time difference between the laser pulse (determined with a photo-diode trigger) and the sense wire signal. Thus, drift velocities and diffusion coefficients can be determined at a variety of pressures, drift fields and magnetic fields.

3. Analysis

To first order (that is, assuming a point source of drift electrons and an infinitesimal slit width), one can integrate Eq. (1) over an infinitely long slit and show the number of electrons which pass through the slit subsequent to the drift to be
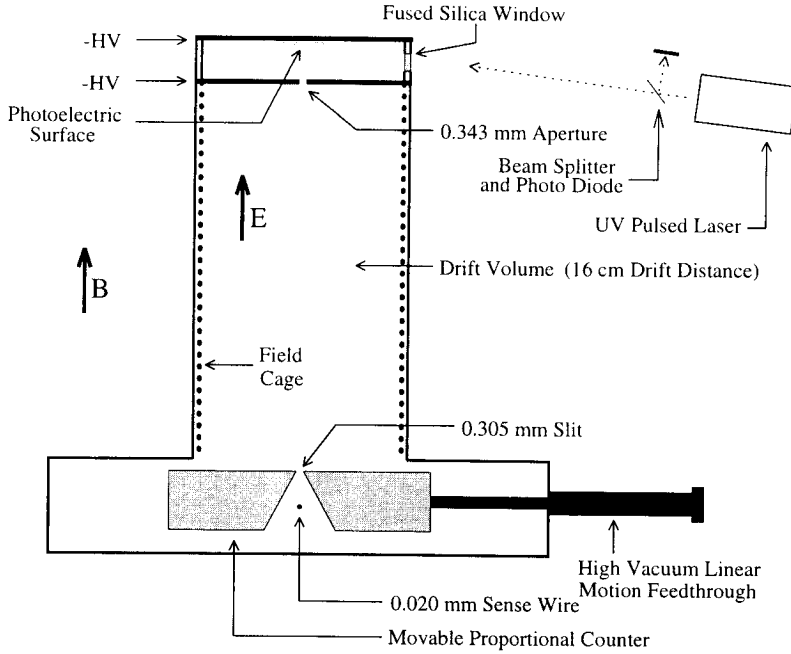
$$\frac{dN}{dx} = N_0 e^{-(x-\mu)^2/2\sigma^2}, \tag{5}$$

Fig. 1. Schematic of device used to measure diffusion coefficient.

where N_0 is a normalization constant and μ is the mean of the diffusion distribution. However, when the diffusion width σ becomes comparable to the slit width and entrance aperture diameter, this approximation breaks down and one must integrate Eq. (5) over the area of the aperture and slit width. The electron distribution after drift then becomes

$$\frac{dN}{dx} = N_0 \int_{x-\varepsilon/2}^{x+\varepsilon/2} dx' \int_{-r}^{r} dr' \left[\mathrm{erf}\,(z_+) - \mathrm{erf}\,(z_-) \right], \quad (6)$$

$$z_\pm = \frac{1}{\sqrt{2}\,\sigma} \left(x' \pm \sqrt{r^2 - r'^2} - \mu \right)$$

where ε is the width of the slit, x is the slit position, and r is the radius of the entrance aperture. (We still assume an infinitely long slit, as this has no significant effect on the final result.)

A typical data run measures the number of counts generated at the proportional wire in 2500 laser pulses at each of roughly 20 slit positions set to effectively define the diffusion profile. However, due to the finite response time of the amplifier, two or more electrons can result in a single discriminator pulse. Therefore,

the intensity of the laser is attenuated to levels that mostly provide either one or zero detected electrons per pulse. A small ($\lesssim 10\%$) Poisson correction is also made to the count totals to compensate for multiple counting, such that if N discriminator pulses are counted, the expected number of electrons is then

$$N' = N_p \ln \left(\frac{N_p}{N_p - N} \right), \quad (7)$$

where $N_p = 2500$ laser pulses. These data are then fit to the functional form given by Eq. (6) using a standard Levenberg–Marquardt method and values of the diffusion width parameter σ are obtained. Typical results are shown in Fig. 2, which displays the data and the result of the fit. Due to the finite aperture size and slit width, the apparent width of the distribution is larger than the width obtained from the fit.

The drift velocity is determined by measuring the time between the laser pulse (as determined by the photo diode trigger) and the signal from the proportional counter. A plot of the drift velocity as a function of K can be found in Fig. 3. The diffusion coefficient can then be determined from the diffusion width and drift velocity using Eq. (2).
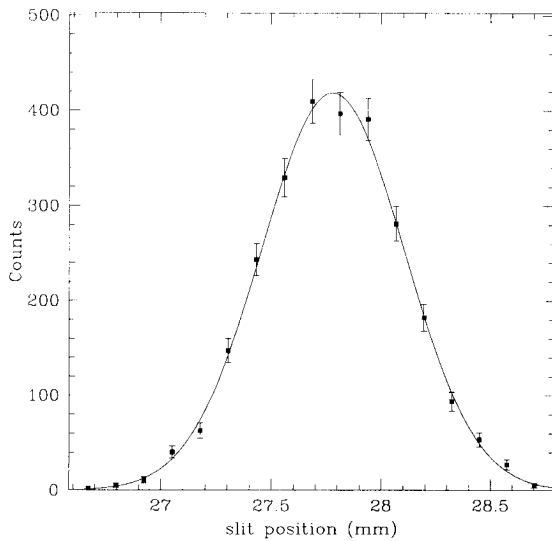
Fig. 2. A typical distribution of drifted electrons. The measurements shown were taken at $K = 1.00$ V/cm/torr, $P = 19.0$ torr, and $B = 3.89$ kG. The fit gives $\sigma = 0.2986 \pm 0.0052$ mm, with χ^2/d.o.f. $= 0.717$. Note that the finite sizes of the aperture and slit width are significant at such a low value of σ. For comparison, fitting the same data to a gaussian distribution gives a value of $\sigma = 0.3229 \pm 0.0048$ mm.
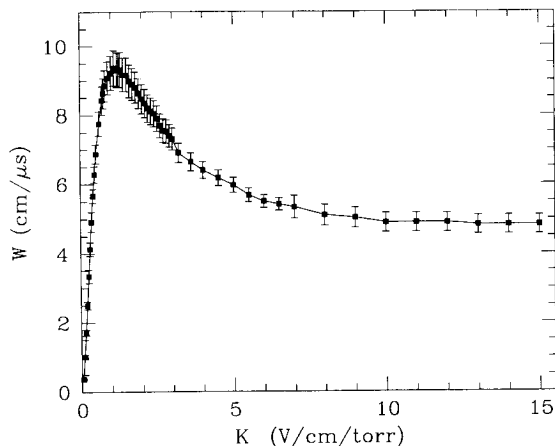

Fig. 3. Drift velocity in methane as a function of K. The points above $K = 3.0$ V/cm/torr were taken at $P = 19$ torr, and the points below $K = 3.0$ V/cm/torr were taken at $P = 95$ torr. (The longitudinal diffusion becomes quite large with $P = 19$ torr at low values of K, introducing a large uncertainty in the drift time.) The error bars shown represent estimates of the systematic error in measuring the drift time due to uncertain rise times in the sense wire amplifier and photo-diode trigger.
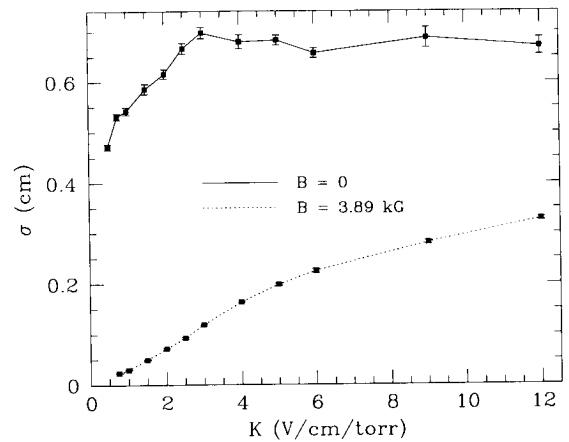

Fig. 4. Diffusion width σ in methane as a function of the reduced electric field K at $P = 19$ torr, with and without a magnetic field. Note that the magnetic field significantly reduces the diffusion width.

4. Diffusion coefficient

The electron transverse diffusion width σ was measured in methane at several pressures between 19 torr and 95 torr and at various values of K. At each pressure, the measurement was made with no magnetic field and with a 3.89 kG magnetic field oriented parallel to the drift field. We first look at measurements taken at constant P and varying K. Plots of σ versus K at $P = 19$ torr and $P = 95$ torr can be found in Figs. 4 and 5. In each plot data is presented for $B = 0$ and $B = 3.89$ kG. The magnetic field greatly reduces the diffusion width, and this effect is most pronounced at low pressure. In each case, the diffusion width is smallest near $K = 1.0$ V/cm/torr, close to where the drift velocity is highest (see Eq. [2]). The corresponding diffusion coefficients can be seen in Fig. 6 for $B = 0$ and in Fig. 7 for $B = 3.89$ kG.

Note that the error bars in the plots of σ represent the statistical errors from fitting to the theoretical diffusion profile. No attempt is made to account for possible systematic errors due to known temporal variations in the laser pulse intensity and degradation of the photosurface during a data run. Therefore, it is likely that the errors shown are slightly understated.

We now look at data taken at different pressures while holding K constant. A plot of the diffusion coefficient as a function of pressure measured at two values of K with no magnetic field is shown in Fig. 8. It
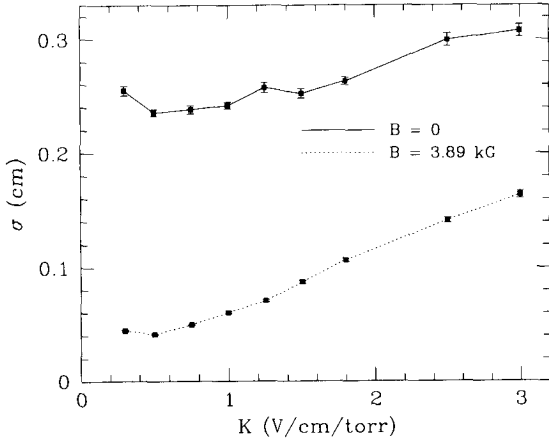
Fig. 5. Diffusion width σ in methane as a function of K at $P = 95$ torr, with and without a magnetic field.
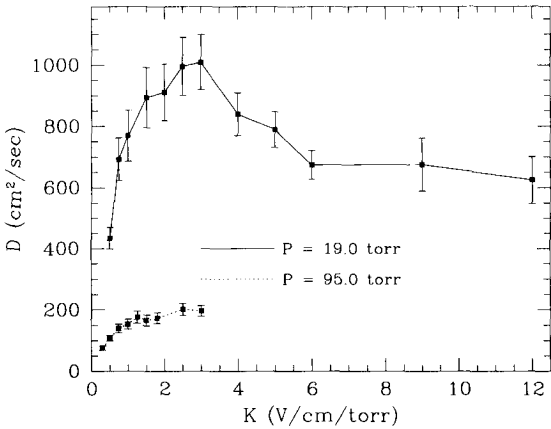

Fig. 6. Diffusion coefficient D in methane as a function of reduced electric field K, at different values of P and with no magnetic field.

can be shown [7] that v is a function of the reduced electric field K, and the electron mean free path is given by

$$l = 1.09 \frac{m}{e} \frac{W}{E} v. \tag{8}$$

Because W is also a function of K [7], we can rewrite Eq. (3) as

$$D = 1.09 \frac{m}{e} \frac{W(K)}{K} \frac{v^2(K)}{3P}, \tag{9}$$
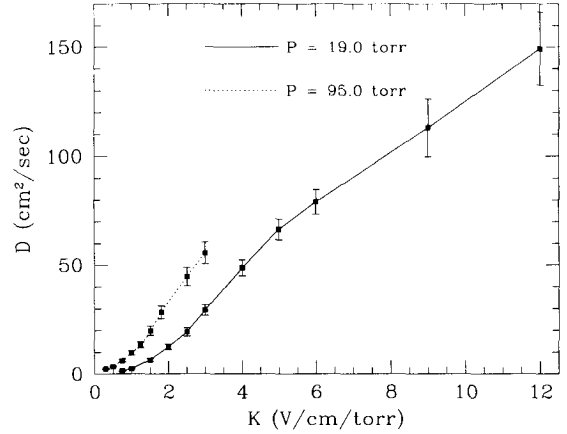
or

$$D = \frac{f(K)}{P}. \tag{10}$$

Fig. 7. Diffusion coefficient D in methane as a function of reduced electric field K, at different values of P and with a 3.89 kG magnetic field oriented parallel to the drift field.

Thus, $D \propto 1/P$ if K is held constant, and this conclusion is supported by the data shown in Fig. 8.

In a strong magnetic field ($\omega\tau \gg 1$), Eq. (4) becomes

$$D(B) = \frac{D(0)}{\omega^2\tau^2}$$

$$= \frac{v^3}{3l\omega^2}$$

$$= \frac{v^2(K)}{3\omega^2} \frac{e}{1.09m} \frac{K}{W(K)} P$$

$$= P \times f(K). \tag{11}$$

Thus, in the presence of a very strong magnetic field parallel to the drift field, $D \propto P$ if K is held constant. Clearly, the diffusion coefficient can be greatly reduced at very low pressures in the presence of only a modest magnetic field. Plots of D as a function of P measured in a $B = 3.89$ kG magnetic field can be seen in Figs. 9 and 10 for $K = 1.0$ V/cm/torr and $K = 3.0$ V/cm/torr respectively. The data for $K = 1.0$ V/cm/torr are consistent with Eq. (11), but for the case of $K = 3.0$ V/cm/torr, a linear relationship is not expected since $\omega\tau \sim 1$. In this case, it can easily be shown that

$$D(B) = \frac{P}{a(K)P^2 + b(K,B)}. \tag{12}$$

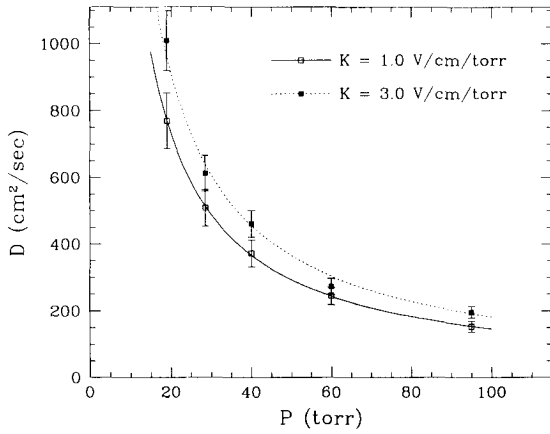As can be seen in Fig. 10, the data are in close agreement with this functional dependence.

Fig. 8. Diffusion coefficient D in methane as a function of gas pressure P, at two values of K and with no magnetic field. The curves shown represent least squares fits to $D = \text{const.} \times P^{-1}$.
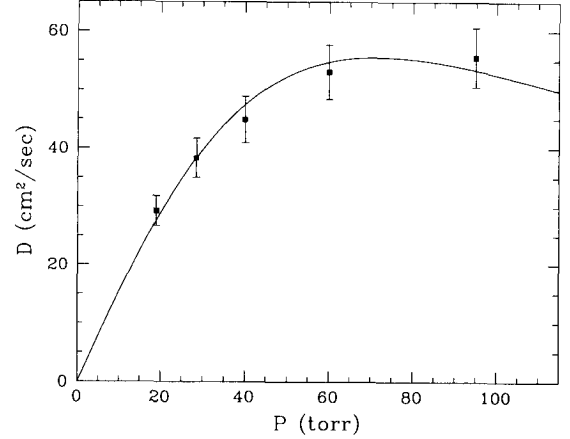

Fig. 10. Diffusion coefficient D in methane as a function of gas pressure P, with $K = 3.0$ V/cm/torr and with a 3.89 kG magnetic field oriented parallel to the drift field. The diffusion coefficients are not linearly related to the pressure since in this case $\omega\tau \sim 1$. However, the data still follow the expected functional dependence as shown by the solid curve, which is a fit to $D = P/(aP^2 + b)$.
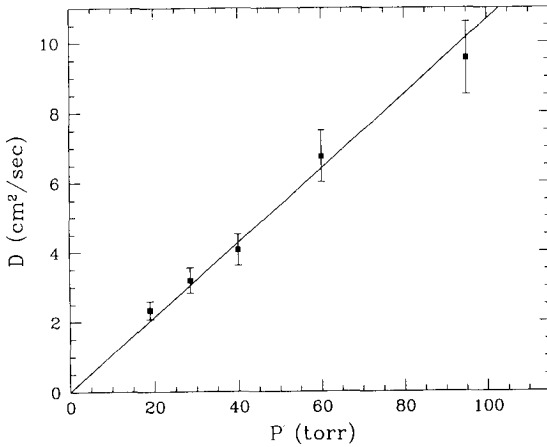

Fig. 9. Diffusion coefficient D in methane as a function of gas pressure P, with $K = 1.0$ V/cm/torr and with a 3.89 kG magnetic field oriented parallel to the drift field. The line shown represents a fit of the data to $D = \text{const.} \times P$.

5. Mean collision times

The electron mean collision time τ determines how well transverse diffusion is suppressed in a magnetic field, and it can be measured in two ways. First, using the drift velocity, we can rewrite Eq. (8) as

$$\tau_W = 1.09 \frac{m}{e} \frac{W}{E}. \tag{13}$$

Alternatively, we can calculate τ from diffusion coefficient measurements taken with and without a mag-
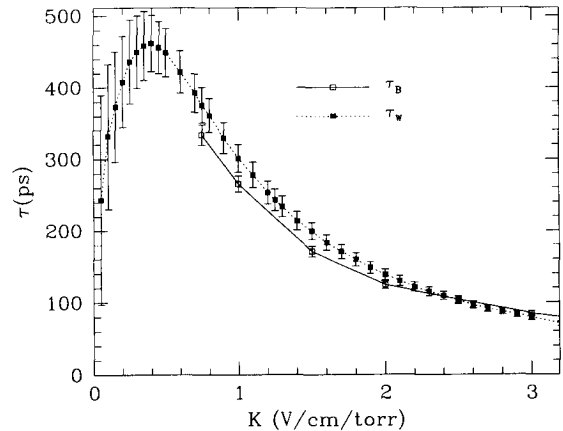

Fig. 11. Mean collision time as a function of K at $P = 19$ torr. The dashed line shows τ_W calculated from the drift velocity, and the solid line shows τ_B as calculated from diffusion coefficients.

netic field by rewriting Eq. (4) as

$$\tau_B = \frac{1}{\omega} \sqrt{\frac{D(0)}{D(B)} - 1}. \tag{14}$$

Plots of τ_W and τ_B versus K can be found in Fig. 11 for $P = 19.0$ torr and in Fig. 12 for $P = 95.0$ torr, and reasonable agreement is shown.

In addition, we can plot τ_W and τ_B versus P at constant values of K, and such plots for $K =$
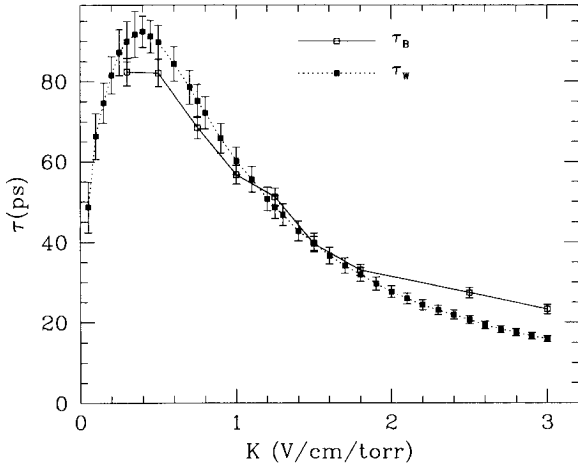
Fig. 12. Mean collision time as a function of K at $P = 95$ torr. The dashed line shows τ_W calculated from the drift velocity, and the solid line shows τ_B as calculated from diffusion coefficients.
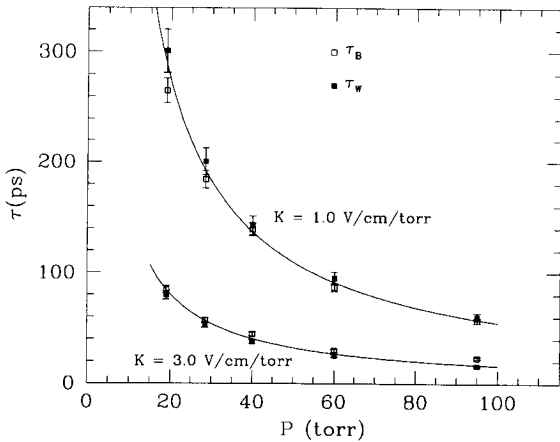

Fig. 13. Mean collision time as a function of P at two values of K. The curves represent least squares fits to $\tau = $ const. $\times$ P^{-1}.

1.0 V/cm/torr and $K = 3.0$ V/cm/torr can be found in Fig. 13. If we rewrite Eq. (13) as

$$\tau = 1.09 \frac{m}{e} \frac{W(K)}{KP}, \tag{15}$$

we see that $\tau \propto P^{-1}$ if K is held constant. This behavior is clearly seen in Fig. 13.

6. Application to low pressure TPC

Previous Monte Carlo simulations of the TPC as a WIMP detector and tests of the performance of the device indicated that the operation of the detector is optimized at a pressure near 19 torr [5,6]. The minimum diffusion width measured at $P = 19$ torr in a 3.89 kG magnetic field (see Fig. 4) is $\sigma = 0.2330 \pm 0.0047$ mm at $K = 0.75$ V/cm/torr. If we extrapolate this width to a drift distance of 114 cm and a $B = 4.5$ kG field, we obtain $\sigma = 0.604 \pm 0.011$ mm, giving a FWHM = 1.42 mm. (Note that while this is the minimum diffusion width that we measured over the probed parameter space, with our current TPC geometry the resolution of the detector is dominated by effects other than diffusion.) The other factor affecting the resolution of an ionization track is the number of electrons N which are detected subsequent to the drift. The actual resolution thus scales as $\sigma/\sqrt{N}$, and tests of the TPC have shown that the ionization density is sufficiently high that the limiting resolution due to diffusion alone can be significantly better than 1 mm.

7. Conclusion

We have presented measurements of diffusion coefficients, drift velocities and electron collision times, and we have shown that these quantities follow the expected functional dependence in the low pressure regime. We have also shown that the transverse diffusion coefficient can be greatly reduced by a magnetic field parallel to the drift, and this effect is most pronounced at low pressures. Given the operating conditions of the TPC to be used in the dark matter search, we can extrapolate the results of this experiment to show that the ionization can be drifted the entire 114 cm length of the TPC and still maintain resolution better than 1 mm.

References

[1] V. Trimble, Existence and Nature of Dark Matter in the Universe, Annual Review of Astronomy and Astrophysics 25 (1987) 425–472.

[2] G.Jungman, M. Kamionkowski and K. Griest, Supersymmetric Dark Matter, Physics Reports 267 (5–6) (1996) 195–373.

[3] J.R. Primack, D. Seckel and B. Sadoulet, Detection of Cosmic Dark Matter, Annu. Rev. Nucl. Part. Sci. 38 (1988) 751–807.

[4] P.F. Smith and J.D. Lewin, Dark matter detection, Phys. Rep. 187 (5) (1990) 203–280.

[5] K.N. Buckland, M.J. Lehner, G.E. Masek and M. Mojaver, Low Pressure Gaseous Detector for Particle Dark Matter, Phys. Rev. Lett. 73 (8) (1994) 1067–1070.

[6] K.N. Buckland, M.J. Lehner and G.E. Masek, Detection of Neutron-Induced Nuclear Recoils in a Low-Pressure Gaseous Detector for Particle Dark Matter Searches, IEEE Trans. Nucl. Sci. 44 (1) (1997) 6–13.

[7] J.S.E. Townsend, Electrons in Gases (Hutchinson's Scientific and Technical Publications, London, 1948).

[8] D. Nygren, The Time-Projection Chamber, PEP-198, 1975.

[9] G.A. Massey, S.H. Bowersox, S. Ghamaty and A. Rahbar, Nonlinear photoemission from organic cathodes excited by a pulsed near-ultraviolet laser, IEEE J. Quantum Electron. (1987).